Journal of chemical & engineering data

Cite This: J. Chem. Eng. Data XXXX, XXX, XXX−XXX

Article

pubs.acs.org/jced

Effective Removal of Humic Acid from Aqueous Solution in an Al-Based Metal−Organic Framework

Xudong Zhao,*[,†] Ting Wang,[†] Guohua Du,[†] Meiqi Zheng,[†] Shuangxue Liu,[†] Zhuoya Zhang,[†] Yuezhong Zhang,[†] Xinli Gao,[‡] and Zhuqing Gao*[,†]

[†]College of Chemical and Biological Engineering and [‡]Instrumental Analysis Center, Taiyuan University of Science and Technology, Taiyuan 030024, China

Supporting Information

ABSTRACT: The adsorption of humic acid (HA) onto an Al^{3+}-based metal−organic framework (MIL-68(Al)) was investigated. MIL-68(Al) was synthesized and characterized using powder X-ray diffraction pattern, Fourier transform infrared spectroscopy, N_2 adsorption−desorption, scanning electronic microscopy, and X-ray photoelectron spectroscopy. Adsorption of HA onto MIL-68(Al) was investigated systematically under various conditions. Experimental results indicate that the adsorption kinetics follow a pseudo-second-order model and adsorption can reach equilibrium at ∼15 min. The adsorption isotherm can be well-fitted with Freundlich model, and the adsorption capacity (115.5 mg g^{-1}) is much higher than those of chitosan, fly ash, activated carbon, etc. Thermodynamic study indicates that the adsorption of HA can be enhanced under lower temperature based on the negative value of adsorption enthalpy (−10.52 kJ mol^{-1}). Besides, MIL-68(Al) can exhibit a high adsorption capacity of 28.53 mg g^{-1} in a real water sample from Fenhe River. The adsorption mechanism can be well-explained by electrostatic interaction and the H-bond interaction. Therefore, this work may provide a guideline to construct MOF-based adsorbents for the high-efficiency capture of HA.

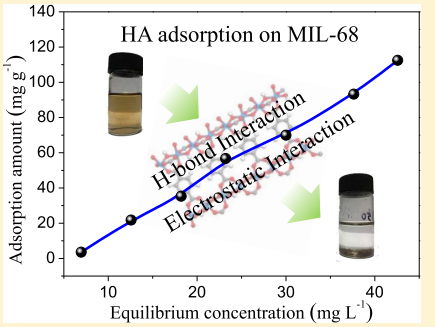

1. INTRODUCTION

Nowadays, water pollution has received increasing attention due to its serious damage to human health and environmental safety. In particular, humic acid (HA), a natural organic compound, is the main cause of water color and odor.[1,2] Additionally, carcinogenic byproducts generated from reaction of HA and chlorine during disinfection process can lead to a serious threat to human health.[3] Therefore, efficient removal of HA from water is necessary. Till date, removal technologies involve various processes, for example, membrane separation, coagulation, and adsorption method.[4−6] Among the developed methods, adsorption method was widely used due to its easy operation, low equipment cost, and high removal efficiency.[7−11] The key for this method is to develop high-efficiency adsorbents especially for porous materials.

Metal−organic frameworks (MOFs) represent a class of solid-state hybrid compounds consisting of metal ions and organic ligands. Thanks to high surface areas, chemical stability, and abundant and designable adsorption sites, MOFs have been considered as promising materials for removing/separating hazardous pollutants from wastewater, such as heavy-metal cations, anions, and organic pollutants,[12−18] whereas the adsorption of HA onto MOFs was rarely reported to date.[19] As an adsorbate, HA contains abundant organic functional groups such as −OH and −COOH; more importantly, HA can exist in aqueous solution in the anionic form of HA-COO^- via the ionization of −COOH. These properties suggest the introduction of H-bond interaction and electrostatic interaction may be proper approaches to achieve high-efficiency capture of HA from aqueous solutions.

Here, we focused on the adsorption of HA onto an Al^{3+}-based metal−organic framework, MIL-68(Al). MIL-68(Al) exhibits strong positive charges surrounded its framework surface at a wide pH range; besides, abundant O sites (C−O−Al) and OH sites (Al−O(H)−Al) can be found in the inorganic cluster, $AlO_4(OH)_2$. These features endow MIL-68(Al) as an ideal material to adsorb HA. As a proof, adsorption isotherm, kinetics and thermodynamics were investigated to evaluate the adsorption performance of MIL-68(Al). Additionally, the effect of solution pH as well as adsorption mechanism was studied systematically. At last, adsorption in a real water sample was studied to confirm the practical use of MIL-68(Al).

2. MATERIALS AND METHODS

2.1. Chemicals. The chemicals including aluminum chloride hexahydrate ($AlCl_3·6H_2O$), terephthalic acid (H_2BDC), *N*,*N*′-dimethylformamide (DMF), methanol, and HA were purchased commercially. The CAS registry nos., suppliers, and mass fractions purities are listed in Table 1. All

Received: May 2, 2019
Accepted: July 2, 2019

Table 1. CAS Registry Number, Mass Fraction Purity, and Suppliers of the Chemicals

chemicals	CAS reg. no.	suppliers	mass fraction purity
aluminum chloride hexahydrate	7784-13-6	HWRK Chem. Co., Ltd.	99%
terephthalic acid	100-21-0	HWRK Chem. Co., Ltd.	99%
N,N′-dimethylformamide	68-12-2	HWRK Chem. Co., Ltd.	>99.5
methanol	67-56-1	HWRK Chem. Co., Ltd.	>99.5
humic acid	1415-93-6	HWRK Chem. Co., Ltd.	98%

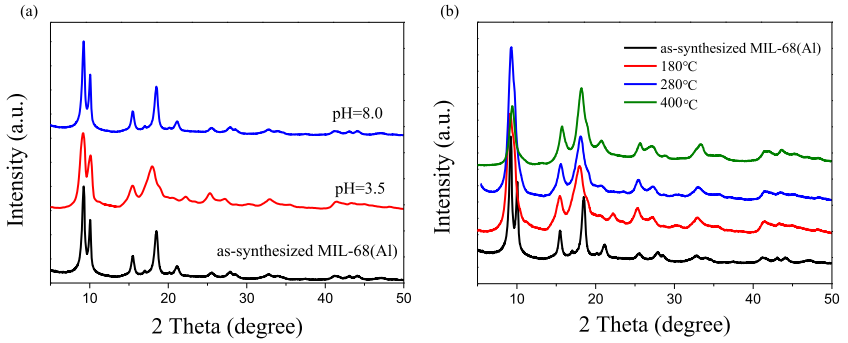

Figure 1. PXRD patterns of MIL-68(Al) under (a) different pH and (b) temperatures (conditions: (a) immersion time: 12 h; (b) heating time: 6 h).

of the chemicals were used directly without further purification.

2.2. Synthesis Procedure. In a typical solvothermal reaction,[20] $AlCl_3{\cdot}6H_2O$ (4.88 g), terephthalic acid (5.0 g), and DMF (300 mL) were added into a 500 mL round-bottom flask and further mixed for 5 min. Then, the system was reflexed at 403 K for 18.5 h. After being cooled down to room temperature, the mixture was filtered, and white solid was collected. In the activation process, the resulting solid was washed with DMF and methanol for two times, respectively. At last, the solid was dried in an oven at 393 K overnight.

2.3. Characterization Techniques. The powder X-ray diffraction (PXRD) patterns of MIL-68(Al) were recorded on a D8 Advance X diffractometer equipped with Cu Kα radiation (λ = 1.54178 Å) at room temperature. The 2θ range from 5 to 50° was scanned with a step size of 0.02°. Nitrogen adsorption−desorption measurements at 77 K were performed on an Autosorb-iQ-MP surface area analyzer. The morphology of MIL-68(Al) was characterized using a Hitachi S-4700 field emission scanning electron microscope (SEM). The Fourier transform infrared (FT-IR) spectra were recorded on a Nicolet iS50 FTIR spectrophotometer. The ζ-potentials of MIL-68(Al) at pH range of 3−8 were measured on a Zetasizer Nano ZS ζ-potential analyzer. Additionally, X-ray photoelectron spectroscopy (XPS) data were collected using an ESCALAB 250 X-ray photoelectron spectroscopy and Al Kα X-ray was selected as the excitation source.

2.4. Adsorption Experiments. All of the adsorption experiments in this work were performed at the batch mode. In a typical adsorption process, MIL-68(Al) (5 mg) was added in the aqueous solution (10 mL) of HA with certain concentrations. After sonication for seconds, the suspension was stirred at 303 K for 12 h in a constant temperature shaker. Then, a centrifugation operation (7000 rpm, 3 min) was performed to separate the suspension. The collected clear solution was used to measure the concentration of HA in a UV−vis spectroscopy. The adsorption capacity was calculated according to eq 1

$$Q = \frac{(C_0 - C_e) \times V}{m} \quad (1)$$

where Q (mg g^{-1}) is the adsorption capacity for HA, C_0 (mg L^{-1}) and C_e (mg L^{-1}) are the initial and final concentrations of HA, respectively, m (g) is the adsorbent mass, and V (L) is the volume of aqueous solution. To confirm the veracity of the data, all of the adsorption experiments were repeated for two or three times.

3. RESULTS AND DISCUSSION

3.1. Characterization Results. The PXRD pattern of the as-synthesized sample was first measured. As shown in Figure 1a, the main characteristic diffraction peaks of the sample can be found at 9.2, 10.0, 15.5, 18.5, and 21.2°, consistent with the data in the reported literatures,[20,21] demonstrating successful synthesis of MIL-68(Al). The chemical stability of MIL-68(Al) was further investigated. From Figure 1a, the main characteristic diffraction peaks of MIL-68(Al) remain intact at the pH of 3.5 and 8.0. At pH = 1.0, the characteristic peaks of MIL-68(Al) disappeared completely (Figure S1), and the new diffraction peaks are assigned to the ligand H_2BDC,[22] indicating the decomposition of MIL-68(Al); at pH = 10.0, there appeared many new peaks in the PXRD pattern (Figure S1), indicating the crystal of MIL-68(Al) experiences a large change. These indicate that MIL-68(Al) can keep stable at pH range of 3.5−8.0. Figure 1b shows the PXRD patterns of MIL-68(Al) at temperature range of 180−400 °C. It can be found that most of characteristic diffraction peaks can remain unchanged after being heated at 180, 280, and 400 °C, demonstrating MIL-68(Al) can be stable up to 400 °C. Overall, the good chemical and thermal stabilities endow this material with potential in liquid-phase adsorption. The SEM image (Figure S2) illustrates that MIL-68(Al) consists of long-strip particles with the length of 100−500 nm. After adsorption of HA, it is obvious that MIL-68(Al) particles were reunited by the introduction of HA molecules.

The porosity of the as-synthesized MIL-68(Al) was evaluated by N_2 adsorption−desorption isotherms measure-

DOI: 10.1021/acs.jced.9b00387
J. Chem. Eng. Data XXXX, XXX, XXX−XXX

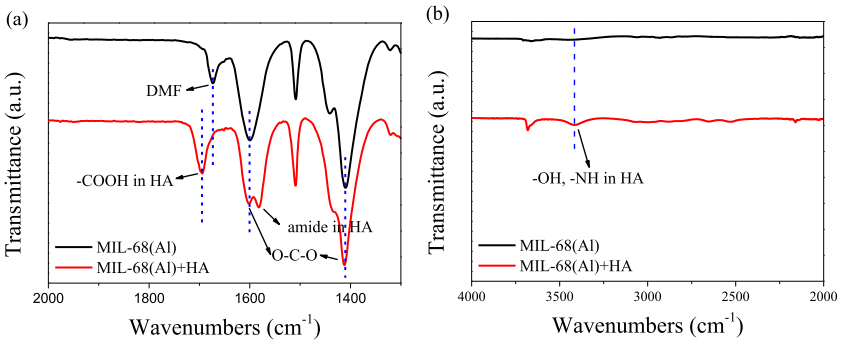

Figure 2. (a, b) FT-IR spectra of MIL-68(Al) before and after the adsorption of HA.

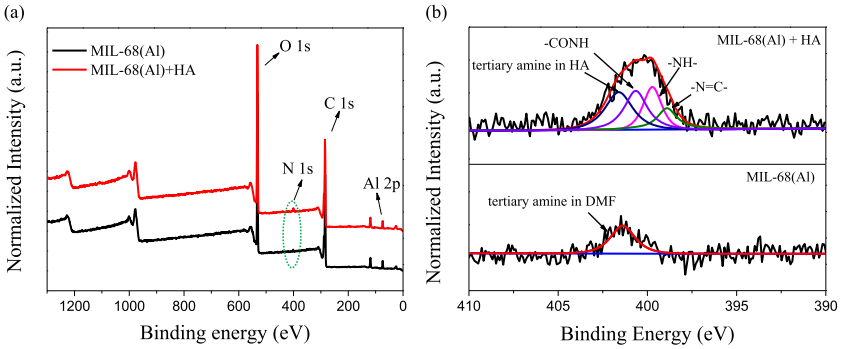

Figure 3. (a) XPS images of MIL-68(Al) before and after the adsorption of humic acid. (b) High-resolution XPS spectra for N 1s.

ment at 77 K (Figure S3). The Brunauer−Emmett−Teller-specific surface area of the sample was calculated to be 1023 m^2 g^{-1}, similar to that in the previous works.[20,23] After the adsorption process, the surface of MIL-68(Al) was coated by the adsorbed HA molecules, which blocked the pores and further resulted in the decreased specific surface area (234 m^2 g^{-1}). In the FT-IR spectrum of the original MIL-68(Al) (Figure 2a), the bands at 1599 and 1409 cm^{-1} are assigned to the stretching vibration of the carboxylate (O−C−O), resulting from the coordination of Al^{3+} and H_2BDC; the peak at 1683 cm^{-1} is assigned to the residual DMF. After the adsorption of HA, the peaks for O−C−O can still be found, demonstrating the stability of the framework of MIL-68(Al); the peak for DMF disappeared, indicating that the residual DMF was washed out in the adsorption process; besides, in the FT-IR spectrum of the HA-loaded MIL-68(Al), the new peaks for −OH, −NH (3414 cm^{-1}), −COOH (1700 cm^{-1}), and −CONH (1582 cm^{-1}) can be found (Figure 2a,b),[24,25] confirming the adsorption of HA onto MIL-68(Al).

Figure 3a shows XPS spectra of MIL-68(Al) before and after the adsorption of HA. The peaks for Al 2p, C 1s, N 1s, and O 1s can be found in the two spectra. As shown in Figure 3a,b, after HA is adsorbed, the peak for N 1s turned stronger and an obvious shift of binding energy can be found. In the high-resolution XPS spectrum for N 1s of the original MIL-68(Al), there is only a peak at 401.08 eV, attributed to the tertiary amine of the residual DMF.[26] After the adsorption of HA, the high-resolution XPS spectrum for N 1s shows four peaks at 398.88, 399.68, 400.78, and 401.68 eV, corresponding to −C−N═C−, −C−NH−C−, −CONH, and tertiary amine, respectively.[27−29] Considering that DMF does not exist in the HA-loaded sample, we suggest the tertiary amine belongs to HA. These results further demonstrate the adsorption of HA onto MIL-68(Al).

At last, the electric property of MIL-68(Al) surface was investigated. As shown in Figure 4, the surface of MIL-68(Al)

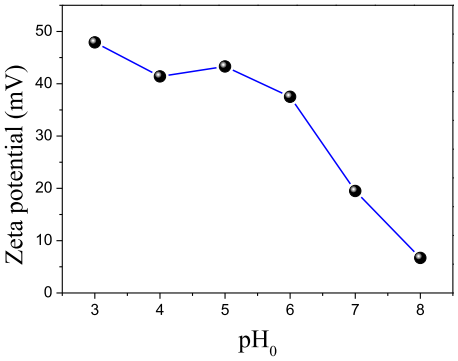

Figure 4. ζ-Potentials of MIL-68(Al) in the aqueous solutions with different pH values.

is positively charged at the pH range of 3.0−8.0, which is mainly attributed to the protonation of −C−O−Al bond (−C−O−Al → −C−OH^+−Al). The ζ-potential decreases gradually with the increasing pH due to the lower protonation degree at higher pH.

3.2. Adsorption of HA on MIL-68(Al). Based on the above conclusion, MIL-68(Al) has good chemical stability, high specific surface area, positively charged surface, and abundant interaction sites. Therefore, in this work, we used this material to remove HA from aqueous solution. The performance was first evaluated by adding 10 mg of MOF sample into 10 mL of HA solution. After 1 h, obvious changes can be observed in both HA solution and MOF sample. From Scheme 1, the HA solution turned from yellowish-brown to almost colorless; meanwhile, white MIL-68(Al) shifted to

DOI: 10.1021/acs.jced.9b00387
J. Chem. Eng. Data XXXX, XXX, XXX−XXX

Scheme 1. Practical Image of HA Adsorbed onto MIL-68(Al) (Condition: C_0, 50 mg L^{-1}; T, 303 K; t, 1 h; Natural pH)

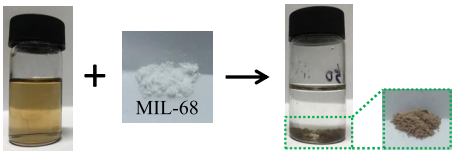

yellowish-brown. These results indicate that MIL-68(Al) has potential in the adsorption of HA from aqueous solution.

3.2.1. Adsorption Kinetics. To systematically study the adsorption performance of MIL-68(Al), adsorption capacity at different times were first measured. As shown in Figure 5,

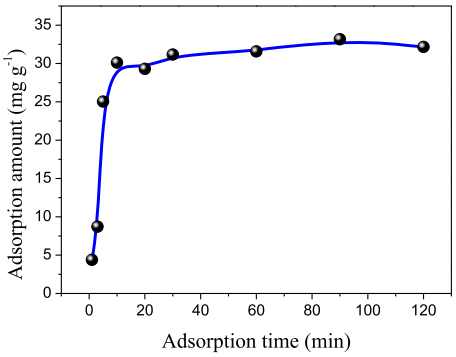

Figure 5. Adsorption capacity of MIL-68(Al) versus time (conditions: C_0, 25 mg L^{-1}; T, 303 K; natural pH).

adsorption can reach an equilibrium at only ~15 min. In general, the adsorption rate is influenced by the availability of surface adsorption sites of adsorbents and the charges of both adsorbents and adsorbates.[30] In this work, MIL-68(Al) owns abundant surface sites, which can interact with HA via H-bond interaction; meanwhile, a strong electrostatic interaction exists between the positively charged surface of MIL-68(Al) and anionic HA-COO^- (see Section 3.2.4 for details). These features contributed to the fast adsorption.

To further study the adsorption kinetics of MIL-68(Al), four kinetic models including pseudo-first/second-order model, Weber and Morris intraparticle diffusion model, and Bangham model (see the Supporting Information for detailed description)[31−34] were used to fit the adsorption data. From the fitting results in Figure S4 and Table 2, the coefficients of determination value R^2 of pseudo-second-order model (0.9967) is superior to those of other models; besides, the calculated adsorption capacity ($Q_{e,cal}$ = 33.67 mg g^{-1}) from the pseudo-second-order model is close to the experimental data (33.02 mg g^{-1}). These demonstrate that the adsorption kinetic data of MIL-68(Al) can be fitted better with the pseudo-second-order model, which revealed that the rate-limiting step in the adsorption process of MIL-68(Al) for HA may be a chemisorption process.[22,35]

3.2.2. Adsorption Isotherm. To evaluate the adsorption capacity of MIL-68(Al) for HA, the adsorption isotherm was recorded as shown in Figure 6. In the initial concentration range of 5−100 mg L^{-1}, the highest adsorption capacity of MIL-68(Al) can reach up to 115.5 mg g^{-1}, which is superior to those of the reported adsorbents such as chitosan, fly ash, activated carbon, and ZIF-8,[19,36−44] as shown in Table 3.

Table 2. Kinetic Model Parameters of HA Adsorbed onto MIL-68(Al)

model	modeling parameters	value
pseudo-first-order	$Q_{e,cal}$(mg g^{-1})	9.57
	k_1 (min^{-1})	0.0287
	R^2	0.6872
pseudo-second-order	$Q_{e,cal}$ (mg g^{-1})	33.67
	k_2 (g min^{-1} mg^{-1})	0.00088
	R^2	0.9967
intraparticle diffusion	k_{id} (mg g^{-1} $min^{-0.5}$)	2.1904
	C	13.74
	R^2	0.4569
Bangham	α	0.4694
	k_0	0.0017
	R^2	0.6914

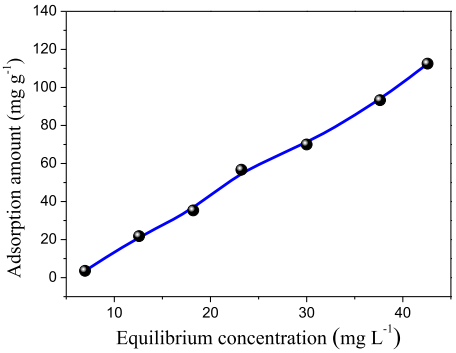

Figure 6. Adsorption isotherm of MIL-68(Al) for HA (condition: C_0, 5−100 mg L^{-1}; T, 303 K; t, 12 h; natural pH).

Meanwhile, the adsorption of HA onto MIL-68(Al) is faster than those of most of the other materials. Although the time of acid-activated Greek bentonite is almost equal to that of MIL-68(Al), the adsorption capacity is much poorer than that of MIL-68(Al).

To understand the adsorption mechanism, several isotherm models were adopted including Langmuir, Freundlich, Dubinin−Radushkevich, and Temkin models (see the Supporting Information for detailed description).[45−48] According to the fitting results (Figure S5 and Table 4), the adsorption data can be fitted better with the Freundlich model than with the other three models. This result revealed the adsorption of HA happened on the heterogeneous surface of MIL-68(Al) caused by the different adsorption sites of itself.[49]

3.2.3. Adsorption Thermodynamics. Adsorption experiments at different temperatures were performed to study the effect of temperature on the adsorption performance of MIL-68(Al). As shown in Figure 7a, the adsorption capacity of MIL-68(Al) decreased with the increasing temperature and maximum adsorption capacity can be obtained at room temperature rather than at higher temperature. Further, to investigate the thermodynamic behavior of HA on MIL-68(Al), thermodynamic parameters including adsorption enthalpy ($\Delta H°$), adsorption entropy ($\Delta S°$), and adsorption Gibbs free energy ($\Delta G°$) were calculated based on the fitting result (Figure 7b) and the equations (see the Supporting Information for a detailed description).[50] From the fitting results in Table 5, $\Delta H°$ was found to be −10.52 kJ mol^{-1}, indicating the exothermic nature of the adsorption process; the negative value of $\Delta S°$ (−24.36 J mol^{-1} K^{-1}) indicates the decreasing randomness. $\Delta G°$ values for 303, 308, 313, 318, and

DOI: 10.1021/acs.jced.9b00387
J. Chem. Eng. Data XXXX, XXX, XXX−XXX

Table 3. Comparison of Maximum Adsorption Capacities of Adsorbents

adsorbents	Q_{max} (mg g^{-1})	C_0 (mg L^{-1})	pH	equilibrium time (min)	T (K)	refs
chitin	27.3	0−80	2.4	25	300	36
chitosan	28.88	0−80	3.07	25	300	36
chitosan-coated activated carbon	68−84[a]		natural pH	∼180	303	37
Fe_3O_4@SiO_2-PANI NP	51.81[a]	4.65−51.15	5.5−6.0	∼600	308	38
RHA	2.7	0−35.0	3−4	60	298 ± 1	39
RHA-NH_2	8.2	0−50.0	3−4	30	298 ± 1	39
magnetic cucurbituril (MQ)	19.10[a]	2−15	7.0	720	308	40
fly ash	10.7[a]	10−100	7.0	6000	303	41
HAP/γ-Fe_2O_3	47.02[a]		7.5	900	298	42
acid-activated Greek bentonite	10.75	10−200		∼15	308	43
graphite	16.5	10−100	5	6000	303	44
ZIF-8	70.2[a]	10−80		∼20	293	19
MIL-68(Al)	115.5	5−100	natural pH	15	303	this work

[a]Capacities from fitting results of Langmuir isotherm model.

Table 4. Isotherm Model Parameters of HA Adsorbed onto MIL-68(Al)

adsorption model	modeling parameter	value
Langmuir	$Q_{m,1}$ (mg g^{-1})	−156.3
	b (L mg^{-1})	0.0064
	R^2	0.8524
Freundlich	k_F [(mg g^{-1})(L $mg^{-1})^{1/n}$]	0.9532
	$1/n$	1.27
	R^2	0.9955
Dubinin−Radushkevich	β_D (mol^2 kJ^{-2})	18819
	$Q_{m,2}$ (mg g^{-1})	81.45
	R^2	0.7981
Temkin	b_T (J mol^{-1})	46.65
	A_T (L g^{-1})	0.144
	R^2	0.9026

Table 5. Thermodynamic Parameters of HA Adsorption onto MIL-68(Al)

T (K)	$\Delta G°$ (kJ mol^{-1})	$\Delta H°$ (kJ mol^{-1})	$\Delta S°$ (J mol^{-1} K^{-1})
303	−3.14	−10.52	−24.36
308	−3.01		
313	−2.89		
318	−2.77		
323	−2.65		

323 K were −3.14, −3.01, −2.89, −2.77, and −2.65 kJ mol^{-1}, respectively, demonstrating that the adsorption of HA onto MIL-68(Al) is spontaneous.

3.2.4. Adsorption Mechanism as well as the Effect of pH. First, from the IR spectra and the XPS analysis for N 1s, it can be confirmed that HA has been adsorbed onto MIL-68(Al). HA contains large number of functional groups such as −OH, −COOH, and −CONH, which can interact with the sites of MIL-68(Al) through H-bond interaction.

More importantly, to the best of our knowledge, electrostatic interaction usually plays an important role on the adsorption of ionic adsorbates on surface-charged adsorbents.[51,52] For the system in this work, the protonation of MIL-68(Al) and the ionization of HA-COOH must be studied in detail. Herein, the two processes were monitored via the change of the solution pH values before and after adsorption (Figure 8a). At pH_0 (initial pH) <5.2, the ionization of HA-COOH was restricted strongly by the low pH_0. pH_f (final pH) was measured to be larger than pH_0, indicating the protonation of MIL-68(Al) rather than the ionization of HA-COOH plays the dominant effect; at pH_0 > 5.2, since the amount of H^+ in solution turns lower, the ionization of HA-COOH rather than the protonation of MIL-68(Al) plays the dominant role, which leads to the lower pH_f than pH_0.

Based on ζ-potential analysis, the surface of MIL-68(Al) is positively charged at the solution pH_0 range of 3.0−8.0. At pH_0 5.2, the ionized HA-COO^- can interact with the protonated MIL-68(Al). At pH_0 > 5.2, with the increase of pH_0, the protonation degree of MIL-68(Al) turns lower, leading to the decreased adsorption capacity (Figure 8b). At pH_0 < 4.1, the ionization degree of HA is weakened, which leads to the weak

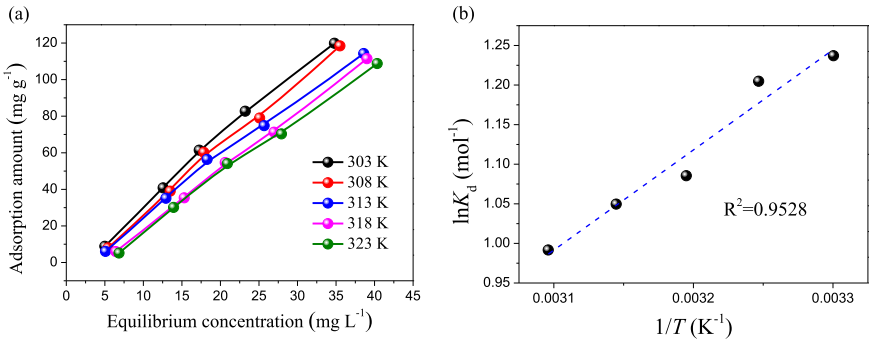

Figure 7. (a) Adsorption capacity of MIL-68(Al) at different temperatures and (b) van't Hoff plot of HA adsorption onto MIL-68(Al) (conditions: C_0, 10−100 mg L^{-1}; t, 12 h; natural pH).

DOI: 10.1021/acs.jced.9b00387
J. Chem. Eng. Data XXXX, XXX, XXX−XXX

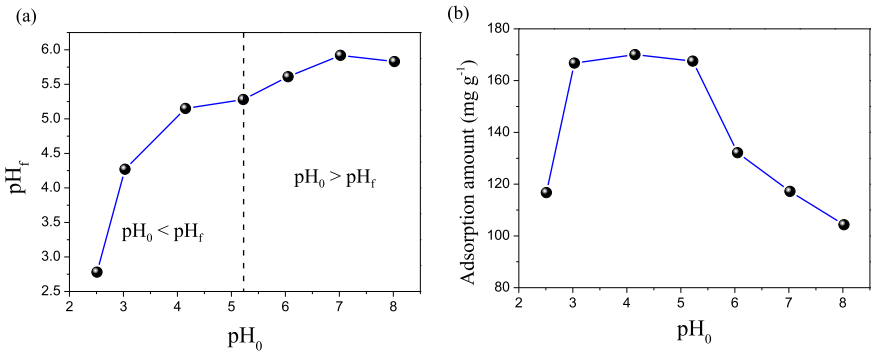

Figure 8. (a) Relation of pH_0 and pH_f. (b) Adsorption capacity at different pH_0.

electrostatic interaction and further poor adsorption capacity (Figure 8b). The adsorption mechanism can be concluded as in Scheme 2.

Scheme 2. Possible Mechanism for Adsorption of HA onto MIL-68(Al)

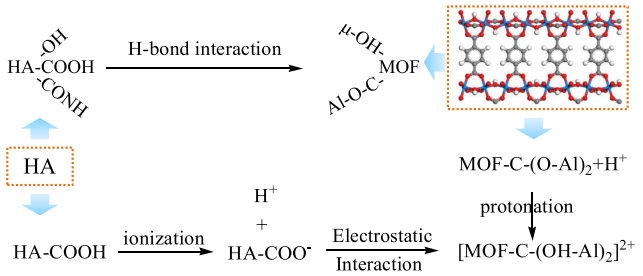

3.2.5. Effect of Coexisting Inorganic Salts. Real aqueous solution of HA commonly contains other coexisting inorganic ions such as Na^+, K^+, NO_3^-, Cl^-, and SO_4^{2-}. From the point of view of practical use, it is necessary to investigate the influence of these coexisting substances. Herein, the concentrations of the salts were consistent to that of HA. As presented in Figure 9, monovalent salts have slightly negative effects on HA

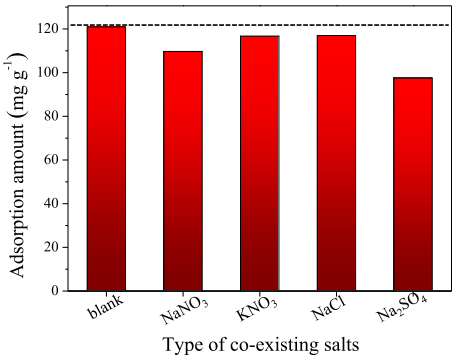

Figure 9. Effect of coexisting inorganic salts on the adsorption of HA onto MIL-68(Al) (condition: C_0, 100 mg L^{-1}; T, 303 K; t, 12 h; natural pH).

adsorption; however, Na_2SO_4 has a relatively larger influence, attributed to its stronger competition for the adsorption sites of MIL-68(Al) than of monovalent salts.

Further, we took a sample from a tributary of Fenhe River (Jinyuan Region, Taiyuan City, Shanxi Province, China). Since there were several solid particles in the water sample, a filtration operation was first performed to obtain the clear solution. The characteristics of the resulting solution can be seen in Table 6. The adsorption capacity of MIL-68(Al) was

Table 6. Characteristics of the Real Water Sample

parameters	result
pH	6.35
conductivity	16 μS cm^{-1}
total phosphorus	2.51 mg L^{-1}
total nitrogen	10.8 mg L^{-1}
sodium	3.62 mg L^{-1}
magnesium	0.81 mg L^{-1}
iron	not detected
calcium	1.21 mg L^{-1}
HA	24.5 mg L^{-1}

measured to be 28.53 mg g^{-1}, comparable to the capacity (33.02 mg g^{-1}) in the solution containing only HA. This result indicates that MIL-68(Al) has good anti-interference ability and may serve as a potential adsorbent to remove HA from real water.

4. CONCLUSIONS

In this work, MIL-68(Al) was introduced for the adsorptive removal of HA from wastewater. The experiment results indicate that a fast adsorption equilibrium (15 min) and high capacity (115.5 mg g^{-1}) can be obtained in MIL-68(Al). Adsorption data can be fitted well with the Freundlich model and pseudo-second-order model. The negative values of adsorption enthalpy (−10.52 kJ mol^{-1}) and adsorption entropy (−24.36 J mol^{-1} K^{-1}) indicate that the adsorption process is an exothermic reaction along with the decreasing randomness. Analysis of the mechanism revealed that electrostatic interaction plays the dominant role in the capture of HA. Furthermore, MIL-68(Al) can exhibit a high adsorption capacity (28.53 mg g^{-1}) in the real water sample from Fenhe River. These results make MIL-68(Al) an potential efficient adsorbent for HA.

■ ASSOCIATED CONTENT

Supporting Information

The Supporting Information is available free of charge on the ACS Publications website at DOI: 10.1021/acs.jced.9b00387.

Models and fitting results of adsorption isotherms, kinetics, and thermodynamics; FT-IR spectra, PXRD patterns, and N_2 adsorption−desorption isotherms of the samples before and after adsorption (PDF)

DOI: 10.1021/acs.jced.9b00387
J. Chem. Eng. Data XXXX, XXX, XXX−XXX

AUTHOR INFORMATION

Corresponding Authors

*E-mail: zhaoxd@tyust.edu.cn (X.Z.).
*E-mail: zqgao2008@163.com (Z.G.).

ORCID

Xudong Zhao: 0000-0001-6035-8758
Zhuqing Gao: 0000-0001-5539-1932

Notes

The authors declare no competing financial interest.

ACKNOWLEDGMENTS

This work was supported by Ph.D. Scientific Research Foundation of Taiyuan University of Science and Technology (Nos. 20162012, 20182020, and 20182058), Key Research Foundation of Science and Technology of Shanxi Province (No. 201803D121099), and Teaching Research and Reform Project of Taiyuan University of Science and Technology (No. ZX20190205).

REFERENCES

(1) An, C.; Yang, S.; Huang, G.; Zhao, S.; Zhang, P.; Yao, Y. Removal of Sulfonated Humic Acid from Aqueous Phase by Modified Coal Fly Ash Waste: Equilibrium and Kinetic Adsorption Studies. *Fuel* **2016**, *165*, 264−271.

(2) Han, S.; Kim, S.; Lim, H.; Choi, W.; Park, H.; Yoon, J.; Hyeon, T. New Nanoporous Carbon Materials with High Adsorption Capacity and Rapid Adsorption Kinetics for Removing Humic Acids. *Microporous Mesoporous Mater.* **2003**, *58*, 131−135.

(3) Lin, J.; Zhan, Y. Adsorption of Humic Acid from Aqueous Solution onto Unmodified and Surfactant-Modified Chitosan/Zeolite Composites. *Chem. Eng. J.* **2012**, *200−202*, 202−213.

(4) Abdullah, N.; Rahman, M. A.; Othman, M. H. D.; Jaafar, J.; Aziz, A. A. Preparation, Characterizations and Performance Evaluations of Alumina Hollow Fiber Membrane Incorporated with UiO-66 Particles for Humic Acid Removal. *J. Membr. Sci.* **2018**, *563*, 162−174.

(5) Xu, H.; Jiao, R.; Xiao, F.; Wang, D. Enhanced Removal for Humic-Acid (HA) and Coagulation Process Using Carbon Nanotubes (CNTs)/Polyalumium Chloride (PACl) Composites Coagulants. *Colloids Surf., A* **2016**, *490*, 189−199.

(6) Thuyavan, Y. L.; Anantharaman, N.; Arthanareeswaran, G.; Ismail, A. F. Adsorptive Removal of Humic Acid by Zirconia Embedded in a Poly(ether sulfone) Membrane. *Ind. Eng. Chem. Res.* **2014**, *53*, 11355−11364.

(7) de Voorde, B. V.; Bueken, B.; Denayer, J.; Vos, D. D. Adsorptive Separation on Metal-Organic Frameworks in the Liquid Phase. *Chem. Soc. Rev.* **2014**, *43*, 5766−5788.

(8) de Andrade, J. R.; Oliveira, M. F.; da Silva, M. G. C.; Vieira, M. G. A. Adsorption of Pharmaceuticals from Water and Wastewater Using Nonconventional Low-Cost Materials: A Review. *Ind. Eng. Chem. Res.* **2018**, *57*, 3103−3127.

(9) ALOthman, Z. A. A Review: Fundamental Aspects of Silicate Mesoporous Materials. *Materials* **2012**, *5*, 2874−2902.

(10) AL-Othman, Z. A.; Ali, R.; Naushad, M. Hexavalent Chromium Removal from Aqueous Medium by Activated Carbon Prepared from Peanut Shell: Adsorption Kinetics, Equilibrium and Thermodynamics Studies. *Chem. Eng. J.* **2012**, *184*, 238−247.

(11) Alqadami, A. A.; Naushad, M.; Alothman, Z. A.; Ahamad, T. Adsorptive Performance of MOF Nanocomposite for Methylene Blue and Malachite Green Dyes: Kinetics, Isotherm and Mechanism. *J. Environ. Manage.* **2018**, *223*, 29−36.

(12) Jiang, D.; Chen, M.; Wang, H.; Zeng, G.; Huang, D.; Cheng, M.; Liu, Y.; Xue, W.; Wang, Z. The Application of Different Typological and Structural MOFs-based Materials for the Dyes Adsorption. *Coord. Chem. Rev.* **2019**, *380*, 471−483.

(13) Peng, Y.; Zhang, Y.; Huang, H.; Zhong, C. Flexibility Induced High-Performance MOF-based Adsorbent for Nitroimidazole Antibiotics Capture. *Chem. Eng. J.* **2018**, *333*, 678−685.

(14) Zhao, X.; Wang, K.; Gao, Z.; Gao, H.; Xie, Z.; Du, X.; Huang, H. Reversing the Dye Adsorption and Separation Performance of Metal-Organic Frameworks via Introduction of -SO_3H groups. *Ind. Eng. Chem. Res.* **2017**, *56*, 4496−4501.

(15) Pi, Y.; Li, X.; Xia, Q.; Wu, J.; Li, Y.; Xiao, J.; Li, Z. Adsorptive and Photocatalytic Removal of Persistent Organic Pollutants (POPs) in Water by Metal-Organic Frameworks (MOFs). *Chem. Eng. J.* **2018**, *337*, 351−371.

(16) Nehra, M.; Dilbaghi, N.; Singhal, N. K.; Hassan, A. A.; Kim, K.-H.; Kumar, S. Metal Organic Frameworks MIL-100(Fe) as an Efficient Adsorptive Material for Phosphate Management. *Environ. Res.* **2019**, *169*, 229−236.

(17) Peng, Y.; Huang, H.; Zhang, Y.; Kang, C.; Chen, S.; Song, L.; Liu, D.; Zhong, C. A Versatile MOF-based Trap for Heavy Metal Ion Capture and Dispersion. *Nat. Commun.* **2018**, *9*, No. 187.

(18) Li, J.; Wang, X.; Zhao, G.; Chen, C.; Chai, Z.; Alsaedi, A.; Hayat, T.; Wang, X. Metal-Organic Framework-based Materials: Superior Adsorbents for the Capture of Toxic and Radioactive Metal Ions. *Chem. Soc. Rev.* **2018**, *47*, 2322−2356.

(19) Lin, K.-Y. A.; Chang, H.-A. Efficient Adsorptive Removal of Humic Acid from Water Using Zeolite Imidazole Framework-8 (ZIF-8). *Water, Air, Soil Pollut.* **2015**, *226*, 1−17.

(20) Yang, Q.; Vaesen, S.; Vishnuvarthan, M.; Ragon, F.; Serre, C.; Vimont, A.; Daturi, M.; Weireld, G. D.; Maurin, G. Probing the Adsorption Performance of the Hybrid Porous MIL-68(Al): A Synergic Combination of Experimental and Modelling Tools. *J. Mater. Chem.* **2012**, *22*, 10210−10220.

(21) Tehrani, M. S.; Zare-Dorabei, R. Competitive Removal of Hazardous Dyes from Aqueous Solution by MIL-68(Al): Derivative Spectrophotometric Method and Response Surface Methodology Approach. *Spectrochim. Acta, Part A* **2016**, *160*, 8−18.

(22) Zhao, X.; Liu, D.; Huang, H.; Zhang, W.; Yang, Q.; Zhong, C. The Stability and Defluoridation Performance of MOFs in Fluoride Solutions. *Microporous Mesoporous Mater.* **2014**, *185*, 72−78.

(23) Xie, L.; Liu, D.; Huang, H.; Yang, Q.; Zhong, C. Efficient Capture of Nitrobenzene from Waste Water Using Metal-Organic Frameworks. *Chem. Eng. J.* **2014**, *246*, 142−149.

(24) Naushad, M.; Ahamad, T.; Al-Maswari, B. M.; Alqadami, A. A.; Alshehri, S. M. Nickel Ferrite Bearing Nitrogen-Doped Mesoporous Carbon as Efficient Adsorbent for the Removal of Highly Toxic Metal Ion from Aqueous Medium. *Chem. Eng. J.* **2017**, *330*, 1351−1360.

(25) Amir, S.; Hafidi, M.; Merlina, G.; Hamdi, H.; Revel, J.-C. Elemental Analysis, FTIR and ^{13}C-NMR of Humic Acids from Sewage Sludge Composting. *Agronomie* **2004**, *24*, 13−18.

(26) Yu, X.; Wang, Z.; Wei, Z.; Yuan, S.; Zhao, J.; Wang, J.; Wang, S. Novel Tertiary Amino Containing Thin Film Composite Membranes Prepared by Interfacial Polymerization for CO_2 capture. *J. Membr. Sci.* **2010**, *362*, 265−278.

(27) Jansen, R. J. J.; van Bekkum, H. XPS of Nitrogen-Containing Functional Groups on Activated Carbon. *Carbon* **1995**, *33*, 1021−1027.

(28) Wu, Z.; Yuan, X.; Zhong, H.; Wang, H.; Jiang, L.; Zeng, G.; Wang, H.; Liu, Z.; Li, Y. Highly Efficient Adsorption of Congo Red in Single and Binary Water with Cationic Dyes by Reduced Graphene Oxide Decorated NH_2-MIL-68(Al). *J. Mol. Liq.* **2017**, *247*, 215−229.

(29) Alqadami, A. A.; Naushad, M.; Alothman, Z. A.; Ghfar, A. A. Novel Metal-Organic Framework (MOF) Based Composites Material for the Sequestration of U(VI) and Th(IV) Metal Ions from Aqueous Environment. *ACS Appl. Mater. Interfaces* **2017**, *9*, 36026−36037.

(30) Deng, H.; Yu, X. Fluoride Sorption by Metal Ion-Loaded Fibrous Protein. *Ind. Eng. Chem. Res.* **2012**, *51*, 2419−2427.

(31) Lagergren, S. Zur Theorie der Sogenannten Adsorption Geloster Stoffe (About the Theory of So-Called Adsorption Soluble Substances), Kungliga Svenska Veten-skapsakademiens. *Handlingar* **1898**, *24*, 1−39.

DOI: 10.1021/acs.jced.9b00387
J. Chem. Eng. Data XXXX, XXX, XXX−XXX

(32) Ho, Y. S.; McKay, G.; Wase, D. A. J.; Foster, C. F. Study of the Sorption of Divalent Metal Ions on to Peat. *Adsorpt. Sci. Technol.* **2000**, *18*, 639−650.
(33) Weber, W. J.; Morris, J. C. Kinetics of Adsorption on Carbon from Solution. *J. Sanit. Eng. Div., Am. Soc. Civ. Eng.* **1963**, *89*, 31−60, DOI: 10.1061/JSEDAI.0000420.
(34) Aharoni, C.; Sideman, S.; Hoffer, E. Adsorption of Phosphate Ions by Colloid Ion-Coated Alumina. *J. Chem. Technol. Biotechnol.* **1979**, *29*, 404−412.
(35) Naushad, M.; Ahamad, T.; Sharma, G.; Al-Muhtaseb, A. H.; Albadarin, A. B.; Alam, M. M.; ALOthman, Z. A.; Alshehri, S. M.; Ghfar, A. A. Synthesis and Characterization of a New Starch/SnO_2 Nanocomposite for Efficient Adsorption of Toxic Hg^{2+} Metal Ion. *Chem. Eng. J.* **2016**, *300*, 306−316.
(36) Ngah, W. S. W.; Musa, A. Adsorption of Humic Acid onto Chitin and Chitosan. *J. Appl. Poly. Sci.* **1998**, *69*, 2305−2310.
(37) Wu, F.-C.; Tseng, R.-L.; Juang, R.-S. Adsorption of Dyes and Humic Acid from Water Using Chitosan-Encapsulated Activated Carbon. *J. Chem. Technol. Biotechnol.* **2002**, *77*, 1269−1279.
(38) Wang, J.; Bi, L.; Ji, Y.; Ma, H.; Yin, X. Removal of Humic Acid from Aqueous Solution by Magnetically Separable Polyaniline: Adsorption Behavior and Mechanism. *J. Colloid Interface Sci.* **2014**, *430*, 140−146.
(39) Imyim, A.; Prapalimrungsi, E. Humic Acids Removal from Water by Aminopropyl Functionalized Rice Husk Ash. *J. Hazard. Mater.* **2010**, *184*, 775−781.
(40) Yang, Q.; Jiang, Y.; Li, X.; Yang, Y.; Hu, L. Magnetic-Supported Cucurbituril: A Recyclable Adsorbent for the Removal of Humic Acid from Simulated Water. *Bull. Mater. Sci.* **2014**, *37*, 1167−1174.
(41) Wang, S.; Zhu, Z. H. Humic Acid Adsorption on Fly Ash and its Derived Unburned Carbon. *J. Colloid Interface Sci.* **2007**, *315*, 41−46.
(42) Shi, M.; Yang, L.; Wei, Z.; Zhong, W.; Li, S.; Cui, J.; Wei, W. Humic Acid Removal by Combining the Magnetic Property of Maghemite with Adsorption Property of Nanosized Hydroxyapatite. *J. Dispersion Sci. Technol.* **2016**, *37*, 1724−1737.
(43) Doulia, D.; Leodopoulos, C.; Gimouhopoulos, K.; Rigas, F. Adsorption of Humic Acid on Acid-Activated Greek Bentonite. *J. Colloid Interface Sci.* **2009**, *340*, 131−141.
(44) Hartono, T.; Wang, S.; Ma, Q.; Zhu, Z. Layer Structured Graphite Oxide as a Novel Adsorbent for Humic Acid Removal from Aqueous Solution. *J. Colloid Interface Sci.* **2009**, *333*, 114−119.
(45) Langmuir, I. The Constitution and Fundamental Properties of Solid and Liquids. Part I. Solids. *J. Am. Chem. Soc.* **1916**, *38*, 2221−2295.
(46) Freundlich, H. M. F. Über Die Adsorption in Lösungen (Over the Adsorption in Solution). *Z. Phys. Chem.* **1906**, *57*, 385−470.
(47) Dubinin, M. M. The Potential Theory of Adsorption of Gases and Vapors for Adsorbents with Energetically Nonuniform Surfaces. *Chem. Rev.* **1960**, *60*, 235−241.
(48) Tempkin, M. J.; Pyozhev, V. Kinetics of Ammonia Synthesis on Promoted Iron Catalyst. *Acta Physicochim. URSS* **1940**, *12*, 327−352.
(49) Wang, T.; Zhao, P.; Lu, N.; Chen, H.; Zhang, C.; Hou, X. Facile Fabrication of Fe_3O_4/MIL-101(Cr) for Effective Removal of Acid Red 1 and Orange G from Aqueous Solution. *Chem. Eng. J.* **2016**, *295*, 403−413.
(50) Alqadami, A. A.; Naushad, M.; Abdalla, M. A.; Khan, M. R.; Alothman, Z. A. Adsorptive Removal of Toxic Dye Using Fe_3O_4-TSC Nanocomposite: Equilibrium, Kinetic, and Thermodynamic Studies. *J. Chem. Eng. Data* **2016**, *61*, 3806−3813.
(51) Alqadami, A. A.; Naushad, M.; Abdalla, M. A.; Ahamad, T.; ALOthman, Z. A.; Alshehri, S. M.; Ghfar, A. A. Efficient Removal of Toxic Metal Ions from Wastewater Using a Recyclable Nanocomposite: A Study of Adsorption Parameters and Interaction Mechanism. *J. Cleaner Prod.* **2017**, *156*, 426−436.
(52) Khan, N. A.; Hasan, Z.; Jhung, S. H. Adsorptive Removal of Hazardous Materials Using Metal-Organic Frameworks (MOFs): A Review. *J. Hazard. Mater.* **2013**, *244*−*245*, 444−456.

DOI: 10.1021/acs.jced.9b00387
J. Chem. Eng. Data XXXX, XXX, XXX−XXX